

**Near-threshold photodetachment of heavy alkali-metal anions**

C. Bahrim

*Department of Physics, Kansas State University, Manhattan, Kansas 66506-2604  
and Department of Chemistry and Physics, Lamar University, Beaumont, Texas 77710-10046*

U. Thumm

*Department of Physics, Kansas State University, Manhattan, Kansas 66506-2604*

A. A. Khuskivadze and I. I. Fabrikant

*Department of Physics and Astronomy, University of Nebraska, Lincoln, Nebraska 68588-0111*

(Received 2 July 2002; published 20 November 2002)

We calculate near-threshold photodetachment cross sections for  $\text{Rb}^-$ ,  $\text{Cs}^-$ , and  $\text{Fr}^-$  using the Pauli equation method with a model potential describing the effective electron-atom interaction. Parameters of the model potential are fitted to reproduce *ab initio* scattering phase shifts obtained from Dirac *R*-matrix calculations. Special care is taken to formulate the boundary conditions near the atomic nucleus for solving the Pauli equation, based on the analytic solution of the Dirac equation for a Coulomb potential. We find a  ${}^3P_1^o$  resonance contribution to the photodetachment cross section of  $\text{Rb}^-$ ,  $\text{Cs}^-$ , and  $\text{Fr}^-$  ions. Our calculated total photodetachment cross sections for Cs agree with experiments after tuning the resonance position by 2.4 meV. For  $\text{Rb}^-$  and  $\text{Fr}^-$  the resonance contribution is much smaller than for Cs. We therefore also provide angle-differential cross sections and asymmetry parameters which are much more sensitive to the resonant contribution than total cross sections.

DOI: 10.1103/PhysRevA.66.052712

PACS number(s): 32.80.Gc, 31.30.Jv

**I. INTRODUCTION**

Recent renewed interest in the processes of photodetachment (PD) of alkali-metal anions [1–3] was caused by the highly increased energy resolution in experimental studies allowing the detection of narrow resonances, Wigner cusps, and other threshold structures in photodetachment processes. Alkali-metal ions are relatively simple systems which can be described at low energies in terms of a two-electron model. Therefore, they are excellent candidates for quantitative comparisons between theory and measurements. Earlier theoretical [4–6] and experimental [7,8] studies were concentrating on the region near the first excitation threshold of neutral atoms where pronounced Wigner cusps were detected.

A recently developed experimental technique combining infrared laser and storage ring experiments allowed observation [9] of the near-threshold behavior of the PD of  $\text{Cs}^-$ . This was direct experimental confirmation of earlier theoretical predictions [10,11] of the  $\text{Cs}^-(6s6p\ {}^3P_1^o)$  resonance state that lies a few meV above the  $\text{Cs}(6s)$  threshold. The existence of this state was a controversial subject for some time. Several theoretical calculations [6,12] predicted first that the  $\text{Cs}^-(6s6p\ {}^3P_J^o)$ ,  $J=0,1,2$ , triplet is slightly bound whereas semiempirical calculations [10,13] based on the analysis of the collisional broadening of Rydberg states by Cs indicated that this triplet should be a resonance state. This controversy was resolved by two independent theoretical works. First, Dirac *R*-matrix calculations of Thumm and Norcross [11] showed that the dielectronic polarization in the  $\text{Cs}^-$  system pushes the  $\text{Cs}^-(6s6p\ {}^3P_J^o)$  states into the continuum. This result was confirmed by independent Breit-Pauli *R*-matrix calculations by Bartschat [14]. Second, Boro-

din, Fabrikant, and Kazansky [15] found that this resonance explains the experimentally observed oscillatory dependence of the cross section for collisional broadening of Rydberg states as a function of the principal quantum number.

This low-energy  ${}^3P^o$  shape resonance exists in all alkali-metal atoms [16] including Fr, as was shown in recent Dirac *R*-matrix calculations [17,18]. However, its experimental observation is very difficult. Although the  ${}^3P^o$  resonance state of  $\text{Rb}^-$  was detected below 50 meV in an electron transmission experiment [19], no direct experimental observations were possible until the recent PD experiment by Scheer *et al.* [9]. Due to the dipole selection rules, only the  $J=1$  component of the  ${}^3P^o$  state can be populated in PD experiments with a single photon. Moreover, since the  ${}^1S^e \rightarrow {}^3P^o$  transition is forbidden in the *LS* coupling scheme, the process indicative of the  ${}^3P^o$  resonance becomes very sensitive to the spin-orbit interaction, and the role of the theory for the interpretation of experimental data becomes especially important.

Most of the previous calculations related to the low-lying spectrum of heavy alkali-metal negative ions are based on scattering models. A comprehensive review of scattering and PD calculations on  $\text{Rb}^-$  and  $\text{Cs}^-$  ions was done by Buckman and Clark [20]. Our recent papers [17,18] attempt to complete this list: see Table II in Ref. [17] and Tables II and III in Ref. [18]. A calculation of resonance states for the  $\text{Fr}^-$  ion was recently done in Refs. [17,18]. To the best of our knowledge, in addition to our recent PD results for  $\text{Cs}^-$  [21], there are no other theoretical PD results available for energies just above the first detachment threshold for  $\text{Rb}^-$ ,  $\text{Cs}^-$ , and  $\text{Fr}^-$  ions. This lack of information was recently pointed out by Scheer *et al.* [9] in connection with their PD experiments on  $\text{Cs}^-$ . This situation is in part due to the difficulties in pro-

viding an accurate treatment of relativistic interactions in quantum calculations for heavy atoms. We are going to address this issue in the present paper, and we will propose an accurate model to treat the spin-orbit interaction in PD of  $\text{Rb}^-$ ,  $\text{Cs}^-$ , and  $\text{Fr}^-$  ions.

Even in a heavy atom, such as Fr, the spin-orbit interaction for valence electrons is relatively weak compared to the Coulomb interaction between them. Therefore the  $^3P_1^o$  resonance should appear in near-threshold PD cross sections as a small “bump” on a smooth background. The background is mainly due to the  $^1P$  contribution which, according to the Wigner threshold law, behaves as  $E^{3/2}$ , where  $E$  is the electron energy in the final state with respect to the PD threshold. This suggests that the spin-orbit interaction can be included in a physically transparent way by using the Pauli equation for the electron in the final state, that is, by adding the term

$$V_{so} = \frac{1}{2c^2} \frac{1}{r} \frac{dV}{dr} \mathbf{s} \cdot \mathbf{l} \quad (1)$$

to the nonrelativistic Coulomb potential  $V$ , and solving the Schrödinger equation with a modified potential for a two-component wave function (the Pauli equation). In Eq. (1) and throughout the paper we use atomic units, unless specified otherwise. However, for a Coulomb potential  $V = -Z/r$ , Eq. (1) leads to a nonphysical  $1/r^3$  singularity near the origin. This singularity does not cause problems if the spin-orbit interaction is treated perturbatively. In this case, the expectation value of the interaction (1) is not divergent for  $l > 0$  because the radial wave function behaves as  $r^l$  near the origin, and for  $l = 0$  it can be shown that the spin-orbit interaction term is identically equal to zero. A more rigorous treatment [22,23], based on the Dirac equation, suggests that the interaction (1) can be regularized by using either the factor  $(1 - V/2c^2)^{-1}$  [4,22] or  $(1 - V/2c^2)^{-2}$  [6,23]. This ambiguity is related to the ambiguity in defining a Hermitian energy-independent Hamiltonian for the Pauli equation when going from two first-order Dirac equations for the large and small components of the relativistic wave function to one second-order Schrödinger-Pauli equation. Such a regularization can be done only in the approximation  $V \ll c^2$ . However, this condition breaks down at distances  $r < Z/c^2$ . This difficulty was addressed in several atomic structure calculations [24] where regular Pauli Hamiltonians were derived and used in self-consistent and many-body calculations of bound states. This problem also should be addressed in calculations of Pauli wave functions for continuum states. In our recent paper [21] we proposed to solve this problem by starting with a Dirac wave function for the detached electron near the origin and introducing a generalization of a well-known transformation [25,26] from the Dirac to the Schrödinger wave function. This allowed us to calculate the  $^3P_1^o$  contribution to PD of  $\text{Cs}^-$ , which is in good agreement with experimental data [9].

In the present paper we give more details about our method and extend our calculations to two other heavy negative alkali-metal ions,  $\text{Rb}^-$  and  $\text{Fr}^-$ . Our results show that  $\text{Cs}^-$  is the anion most favorable for observation of the  $^3P_1^o$

resonance in PD. Although the spin-orbit interaction in  $\text{Fr}^-$  is stronger, the resonance there is broader. Our calculations indicate that it would be difficult to detect experimentally the  $^3P_1^o$  resonance in  $\text{Rb}^-$  and  $\text{Fr}^-$  by measuring *total* PD cross sections. However, angle-differential cross sections and the asymmetry parameter are much more sensitive to the spin-orbit interaction and are calculated in this work in order to provide guidance for future experiments.

This paper is organized as follows. In the next section we explain our method of calculating PD cross sections from the Pauli wave function. In Sec. III, we construct a model potential for the electronic interaction with the neutral atom based on results of Dirac  $R$ -matrix scattering calculations. In Sec. IV, we discuss details of our treatment of the spin-orbit term. Numerical results and their discussion will follow in Sec. V, and we conclude with a brief summary in Sec. VI.

## II. CROSS SECTIONS AND BOUNDARY CONDITIONS

We will calculate PD cross sections by integration of the Pauli equation for one effective electron. The spin-dependent interaction of the active electron with the spin-1/2 alkali-metal atom is represented by a spin-dependent effective potential (see Sec. III below). Parameters in this potential will be adjusted to reproduce the scattering phases provided by previous two-electron Dirac  $R$ -matrix calculations [17,18].

The angle-differential photodetachment cross section is given by

$$\frac{d\sigma}{d\Omega} = \frac{4\pi^2 k \omega}{c} |\hat{\epsilon} \cdot \mathbf{D}_{fi}|^2, \quad (2)$$

where  $k$  is the electron momentum of the detached electron,  $\omega$  the photon frequency,  $\hat{\epsilon}$  the photon polarization vector, and  $\mathbf{D}_{fi}$  the matrix element of the dipole operator. We use the length form of the dipole matrix element which is appropriate for calculations involving model potentials [27].

For linearly polarized light along the  $z$  axis we have

$$\hat{\epsilon} \cdot \mathbf{D}_{fi} = \int \psi_{\mathbf{k}}^{(-)*} z \psi_i d\mathbf{r}, \quad (3)$$

where the complex conjugate of the “minus” solution (incident plane wave  $\phi_{\mathbf{k}}$  plus ingoing wave) can be expressed through the “plus” solution as

$$\psi_{\mathbf{k}}^{(-)*} = \psi_{-\mathbf{k}}^{(+)}$$

The plus solution consists of the incident plane wave  $\phi_{\mathbf{k}}$  and an outgoing wave. We write the plus solution as a linear combination of eigenstates of the total angular momentum quantum numbers  $J$  and  $M_J$ ,

$$\begin{aligned} \psi_{\mathbf{k}SM_S}^{(+)} = & \sum_{LM_L S' J M_J} A_{LM_L S' J M_J}^{JM_J}(\mathbf{k}) \mathcal{Y}_{LS' J M_J}(\hat{r}_1, s_1, s_2) \\ & \times R_{LS' S}^J(r_1). \end{aligned} \quad (4)$$

The arguments  $s_1$  and  $s_2$  represent the spin variables for the detached and atomic electrons, respectively, while  $\hat{r}_1$  represents the angular variables for the detached electron. The atomic electron is in an  $s$  state (e.g.,  $6s$  for Cs) and its wave function does not depend on angular variables. The coupling of the total spin and orbital angular momentum is included in the function

$$\mathcal{Y}_{LS'JM_J}(\hat{r}_1, s_1, s_2) = \sum_{M_L M_S} C_{LM_L S' M_S}^{JM_J} Y_{LM_L}(\hat{r}_1) \chi_{S' M_S}(s_1, s_2), \quad (5)$$

where  $\chi_{S' M_S}(s_1, s_2)$  is the total spin function of the system, and  $C_{LM_L S' M_S}^{JM_J}$  is a Clebsch-Gordan coefficient.  $S$  in Eq. (4) is the final total spin. Generally, we should also consider transitions between states with different values of total orbital angular momentum  $L$ , but in our case the spin-orbit interaction mixes only  $^1P$  and  $^3P$  states since the atomic valence electron is in an  $s$  state and the detached electron's angular momentum is  $l=1$ .

The coefficients  $A_{LM_L SM_S}^{JM_J}(\mathbf{k})$  in Eq. (4) are determined from the boundary condition at  $r_1 \rightarrow \infty$ . Let us look first at the asymptotic behavior of the radial wave function

$$R_{LS'S}^J(r) \sim \frac{1}{r} \sin(kr - L\pi/2) \delta_{S'S} + \frac{1}{r} \exp[i(kr - L\pi/2)] f_{S'S}^J, \quad (6)$$

where  $f_{S'S}^J$  is the scattering amplitude. Substituting this expression into Eq. (4), we obtain for the incident plane wave

$$\phi_{\mathbf{k}SM_S} \sim \sum_{LM_L JM_J} A_{LM_L SM_S}^{JM_J}(\mathbf{k}) \mathcal{Y}_{LSJM_J}(\hat{r}_1, s_1, s_2) \frac{1}{r} \times \sin(kr - L\pi/2). \quad (7)$$

We want this equation to correspond to the partial-wave expansion of a plane wave normalized to the  $\delta$  function of momentum  $\mathbf{k}$ ,

$$\phi_{\mathbf{k}SM_S} = (2\pi)^{-3/2} e^{i\mathbf{k}\cdot\mathbf{r}} \chi_{SM_S}(s_1, s_2). \quad (8)$$

Since  $L$  and  $S$  are uncoupled in Eq. (8), we write  $A$  in the form

$$A_{LM_L SM_S}^{JM_J}(\mathbf{k}) = C_{LM_L SM_S}^{JM_J} B_{LM_L}(\mathbf{k}). \quad (9)$$

Using the explicit expression for  $\mathcal{Y}_{LS'JM_J}$ , Eq. (5), and the orthogonality property for the Clebsch-Gordan coefficients, we obtain

$$\phi_{\mathbf{k}SM_S} \sim \sum_{LM_L} B_{LM_L} Y_{LM_L}(\hat{r}_1) \chi_{SM_S}(s_1, s_2) \frac{1}{r_1} \sin(kr_1 - L\pi/2). \quad (10)$$

Comparing this expression with the partial-wave expansion of the plane wave, Eq. (8), we obtain

$$B_{LM_L}(\mathbf{k}) = \left(\frac{2}{\pi}\right)^{1/2} \frac{i^L}{k} Y_{LM_L}^*(\hat{k}). \quad (11)$$

Finally we have for the partial-wave expansion of  $\psi^{(+)}$ ,

$$\psi_{\mathbf{k}SM_S}^{(+)} = \left(\frac{2}{\pi}\right)^{1/2} \frac{1}{k} \sum_{LM_L} i^L Y_{LM_L}^*(\hat{k}) \sum_{S' JM_J} C_{LM_L SM_S}^{JM_J} \times \mathcal{Y}_{LS'JM_J}(\hat{r}_1, s_1, s_2) R_{LS'S}^J(r_1). \quad (12)$$

$\psi_{\mathbf{k}SM_S}^{(+)}$  can be obtained from here by replacing  $i^L$  by  $i^{-L}$ .

To find the explicit expression for the PD matrix element, we write the initial  $^1S$  state as

$$\psi_i = \frac{1}{\sqrt{4\pi}} \frac{u_b(r)}{r} \chi_{00}(s_1, s_2) \quad (13)$$

and the final-state radial function as

$$R_{LS'S}^J = \frac{1}{r} u_{LS'S}^J. \quad (14)$$

Then for the matrix element, Eq. (3), we obtain

$$\hat{\mathbf{e}} \cdot \mathbf{D}_{fi} = \frac{1}{ik} \left(\frac{2}{3\pi}\right)^{1/2} \sum_{M_L} C_{1M_L SM_S}^{10} Y_{1M_L}^*(\hat{k}) M_S, \quad (15)$$

where  $M_S$  is the radial matrix element

$$M_S = \int u_{10S}^1(r) r u_b(r) dr. \quad (16)$$

For the differential PD cross section into the state with the total spin  $S$  we have

$$\frac{d\sigma_S}{d\Omega} = \frac{8\pi\omega}{3ck} |M_S|^2 \sum_{M_S M_L} |C_{1M_L SM_S}^{10} Y_{1M_L}(\hat{k})|^2. \quad (17)$$

Because of the relative weakness of the spin-orbit interaction, the final channel  $S=0$  can be called *dominant*, and the  $S=1$  channel can be called *weak*. As we can see from Eq. (17), the angular distribution in the dominant channel is given by  $\cos^2\theta$ , where  $\theta$  is the angle between the photon polarization vector and the momentum vector  $\mathbf{k}$ , whereas the angular distribution in the weak channel is given by  $\sin^2\theta$ . Therefore a nonzero value of the differential cross section in the region  $\theta = \pi/2$  is a signature of the spin-orbit interaction. Moreover, this effect should become more pronounced in the vicinity of the  $^3P$  shape resonance.

For the total cross section we get after integration over  $\hat{k}$ ,

$$\sigma_S = \frac{8\pi\omega}{3ck} |M_S|^2, \quad (18)$$

and the observed cross section is obtained by summing over  $S$ .

The matrix  $\mathbf{u}$  of radial functions  $u_{S'S}(r)$  (for  $J=1$  and  $L=1$ ) in Eq. (14) is obtained by numerical integration of

coupled equations. Using the asymptotic boundary conditions Eq. (6), we can write down the matrix  $\mathbf{u}$  in the following form:

$$\mathbf{u} = \frac{i}{2} [\mathbf{u}^{(-)} - \mathbf{u}^{(+)} \mathbf{S}], \quad (19)$$

where  $\mathbf{S}$  is the scattering matrix, and  $\mathbf{u}^{\pm}$  has the following asymptotic form:

$$u_{S'S}^{\pm}(r) \sim \exp[\pm i(kr - \pi/2)] \delta_{S'S}. \quad (20)$$

Together with the regular behavior at the origin, this gives us the boundary conditions for  $\mathbf{u}$ , and uniquely determines  $\mathbf{u}$  as a solution of coupled radial equations [cf. Eq. (36) below].

### III. THE POTENTIAL MATRIX

Since we are interested in near-threshold PD for energies much lower than the  $ns-np_{1/2}$  excitation energy of the neutral atom [ $n=5$  (Rb), 6(Cs), and 7(Fr)], we have chosen to describe the effective interaction of the electron with an alkali-metal atom by an  $LS$ -dependent model potential [6] which is adjusted to reproduce the low-energy scattering eigenphases for  $J \leq 2$  and odd parity obtained from the Dirac  $R$ -matrix calculations [17,18].

According to Ref. [28] two methods for the description of the effective interaction between an electron and a many-electron atom can be distinguished. In the model-potential approach the effective interaction is attractive, and leads to atomic core states and scattering states. In this case, the scattering wave function contains the correct number of nodes, and the phase shifts satisfy the generalized Levinson theorem [29]. In the alternative pseudopotential description, the atomic core states are excluded by introducing a strong repulsive core [30]. For a treatment which should incorporate the spin-orbit interaction, the second method is not acceptable, because the spin-orbit interaction effects are most important at short distances where the electron accelerates to high velocity due to the large nuclear charge. Therefore in the present paper we use the model-potential method.

To describe the effective electron-atom interaction we introduce a separate local potential for each scattering state, defined by the quantum numbers  $L$  and  $S$ ,

$$\hat{V} = \sum_{LS} |LS\rangle V_{LS} \langle LS|. \quad (21)$$

For the  $P$  state of the alkali-metal negative ions, the interaction potential is given by

$$V_{L=1,S}(r) = -\frac{Z}{r} e^{-\lambda r} - A e^{-\gamma r} - \frac{\alpha}{2r^4} [1 - e^{-(r/r_c)^6}] + V_{so}, \quad (22)$$

while the potential for the  $S$  state is

$$V_{L=0,S}(r) = -\frac{Z_S}{r} e^{-\gamma r} - \frac{\alpha}{2r^4} [1 - e^{-(r/r_c)^6}], \quad (23)$$

TABLE I. The fit parameters  $Z_S$ ,  $\lambda$ ,  $A$ ,  $\gamma$ , and  $r_c$  for the model potentials  $V_{L=0,S}(r)$  in Eq. (23) and  $V_{L=1,S}(r)$  in Eq. (22) used to reproduce the scattering phase shifts provided by Dirac  $R$ -matrix calculations [17] together with the nuclear charge  $Z$  and the radius  $r_0$  for the transition to a pure Coulomb potential  $Z/r$  at  $r < r_0$ .

Atom ( $Z$ )	$r_0$	$\lambda$	State	$Z_S$	$A$	$\gamma$	$r_c$
Rb(37)	0.01	7.4975	$^1S^e$	4.5642		1.3438	1.8883
			$^1P^o$		-4.2625	1.0055	1.8869
			$^3P^o$		-1.4523	4.8733	1.8160
Cs(55)	0.014	7.2443	$^1S^e$	4.5396		1.3304	1.6848
			$^1P^o$		-3.6681	1.3195	1.8031
			$^3P^o$		4.1271	2.2329	2.1314
Fr(87)	0.025	7.1607	$^1S^e$	5.2003		6.6603	1.1508
			$^1P^o$		-5.2272	0.60953	1.4891
			$^3P^o$		0.5904	1.9179	1.8919

since the spin-orbit interaction term vanishes. Furthermore,  $Z$  is the nuclear charge,  $\alpha$  the atomic polarizability for the ground state of the neutral atom [319.2 (Rb), 402.2 (Cs), and 317.8 (Fr)], and  $\lambda$  the nuclear screening parameter.  $Z_S$  and  $A$  are two more adjustable parameters. The first two terms in Eq. (22) describe the short-range Coulomb interaction: the first term is a screened Coulomb potential, the second term is an additional screening term due to the atomic electrons, while the third term describes the long-range dipole interaction multiplied by a cutoff function to eliminate the divergence at the origin. The  $P$  state is less penetrating. Therefore, near the nucleus, we use the unscreened Coulomb attractive potential [the first term in Eq. (22)]. For the  $S$  state, the nuclear charge is screened more strongly by inner electrons, and we include the adjustable screened charge  $Z_S$  in Eq. (23). Except for  $\lambda$ , all other fit parameters in Eqs. (22) and (23) depend on  $L$  and  $S$ , and are given in Table I. Since the spin-orbit interaction term vanishes for the  $^1S^e$  state, the first term in Eq. (23) has a weak influence on low-energy electron-atom scattering. In contrast, for the  $^3P^o$  state, the position and width of the  $J$  fine-structure components are very sensitive to the near-nuclear region [especially for the  $\text{Cs}^- (^3P^o)$  resonance], where the interaction (1) is important.

The spin-orbit interaction operator is calculated according to Eq. (1) with the orbital angular momentum and spin operators for the detached electron  $\mathbf{l} = \mathbf{l}_1 = L$  and  $\mathbf{s} = \mathbf{s}_1$ . We do not include the spin-orbit term for the atomic electron since its orbital angular momentum remains 0.

We calculate the matrix elements of the operator  $\mathbf{l}_1 \cdot \mathbf{s}_1$  in the basis  $LSJM_J$ ,

$$D_{SS'}^J = \langle LSJM_J | \mathbf{l}_1 \cdot \mathbf{s}_1 | L' S' J M_J \rangle. \quad (24)$$

Using the Wigner-Eckart theorem in standard  $(J, M_J)$  representation, we can write the matrix elements

$$D_{SS'}^J = (-1)^{J+S+L'} \begin{Bmatrix} L' & S' & J \\ S & L & 1 \end{Bmatrix} \langle L || \mathbf{l}_1 || L' \rangle \langle S || \mathbf{s}_1 || S' \rangle \quad (25)$$

as products of reduced matrix elements and 6- $j$  symbols. The reduced matrix elements are

$$\langle L||\mathbf{1}_1||L'\rangle = \delta_{LL'}\sqrt{L(L+1)(2L+1)} \quad (26)$$

and

$$\begin{aligned} \langle S||\mathbf{s}_1||S'\rangle \\ = (-1)^{S'}\sqrt{\frac{3(2S+1)(2S'+1)}{2}} \begin{Bmatrix} S & 1 & S' \\ 1/2 & 1/2 & 1/2 \end{Bmatrix}. \end{aligned} \quad (27)$$

In the case of interest  $J=L=1$ , and  $S$  and  $S'$  have two possible values, 0 and 1. Calculation of the reduced matrix elements and 6- $j$  symbols in this case gives  $D_{00}^1=0$ ,  $D_{11}^1=-1/2$ , and  $D_{01}^1=1/\sqrt{2}$ .

There are two additional electron scattering channels, which do not contribute directly to PD due to the dipole selection rules, but which were nevertheless considered to fit the parameters of our model potential to the scattering eigenphases provided by our separate Dirac  $R$ -matrix calculation. These channels are characterized by the quantum numbers  $L=1$ ,  $J=0$  and  $L=1$ ,  $J=2$ . The corresponding values of  $D_{SS'}^J$  are  $D_{11}^0=-1$  and  $D_{11}^2=1/2$ . These different values of  $D_{11}^J$  are responsible for the splitting of the low-energy  $^3P$  resonance, similar to the fine-structure splitting of the  $^3P$  states of Ba. Therefore the fit potential parameters in the  $S=1$  channel were taken the same in all scattering symmetries and were fitted to reproduce the splitting between the  $J=0$  and  $J=2$  resonances.

#### IV. TREATMENT OF THE SPIN-ORBIT TERM

Equation (1) contains an unphysical  $1/r^3$  singularity near the origin. It appears due to the approximate treatment of the spin-orbit interaction. The second-order differential equation for the large component of the Dirac wave function contains the term

$$\frac{1}{r} \frac{dV}{dr} \frac{1}{E-V+c^2}, \quad (28)$$

where  $E=c^2+E_{NR}$  includes the electron rest mass and the nonrelativistic energy  $E_{NR}$ . Since  $|E_{NR}|\ll c^2$  and, at  $r\gg Z/c^2$ ,  $|V|\ll 2c^2$ , the denominator  $E-V+c^2$  becomes equal to  $2c^2$ , and Eq. (28) becomes identical with Eq. (1). Thus, Eq. (1) becomes invalid at short distances of the order of  $Z/c^2$ . Although this distance is small (it is still large compared to the size of the nucleus, however), it is important to remove the  $1/r^3$  singularity because it affects the boundary condition at the origin and, therefore, the overall behavior of the wave function.

Our method starts with separating the entire space into two regions: in the inner region, limited by a sphere of radius  $r_0$ , the only important nonrelativistic interaction is the unscreened Coulomb interaction between the detached electron and the nucleus [31]. In this region relativistic interactions (i.e., the spin-orbit interaction for electrons with low angular

momentum and the relativistic mass correction) are important, and the total angular momentum quantum number of the detached electron,  $j$ , is conserved, making the  $jj$  representation a natural choice. For  $r>r_0$ , we neglect terms of order  $Z/(c^2r)$ , i.e., the Coulomb potential energy  $-Z/r$  compared to the electron rest energy  $c^2$ . In this region, the effective potential is not diagonal in the  $jj$  representation because of the exchange effects, and the  $LS$  representation is more appropriate, where, as in the previous section,  $L$  is the total orbital angular momentum and  $S$  is the total spin of the atom + detached electron system. The effective potential is not diagonal in the  $LS$  representation due to spin-orbit interaction effects; however, the off-diagonal elements are small. The parameter  $r_0$  should satisfy simultaneously the following requirements:  $r_0\gg Z/c^2$ , and  $r_0\ll 1/\lambda$ , where  $\lambda$  is the screening parameter in Eq. (22). An order of magnitude estimate for the radius  $r_0$  is 0.01. However, this value does not satisfy these requirements with high accuracy. Indeed, for Cs at  $r=0.01$  the Coulomb  $Z/r$  term is still 29% of the rest energy term  $c^2$  whereas the screening exponential  $\exp(-\lambda r)$  is already 0.93, a noticeable deviation from the pure Coulomb potential. To resolve this difficulty we use the following approach. We postulate that our model potential is equal to the pure Coulomb potential  $Z/r$  at  $r<r_0$  and that only at  $r>r_0$  does it take the form of Eq. (22). This creates a slight discontinuity in  $V_{L=1,S}(r)$ , but does not cause problems in fitting the potential parameters. If a continuous potential is desirable, one can introduce an additional constant factor  $\exp(\lambda r_0)$  at  $r>r_0$ . For  $r>r_0$ , where the Coulomb term is still not negligible compared to the rest energy term, we use the Bethe and Salpeter regularization factor  $(1-V/2c^2)^{-1}$  [22]. The PD cross section is quite insensitive to the exact form of the regularization factor at  $r>r_0$ . In particular, the  $^3P$  contribution to the PD of  $\text{Cs}^-$  decreases only by 1% when we switch from the Bethe-Salpeter to the Condon and Shortly regularization factor  $(1-V/2c^2)^{-2}$  [23] at  $r>r_0$ .

To start the integration of the coupled equations with the model potentials (22) and (23), we use first the well-known solution of the Dirac equation for an electron in the Coulomb potential [26]. The large component  $G_\kappa(r)$  with a very good accuracy is given by the solution for zero nonrelativistic energy

$$G_\kappa(r) = (\kappa - s)J_{2s}(y) + \frac{y}{2}J_{2s+1}(y), \quad (29)$$

where  $s=(\kappa^2-Z^2/c^2)^{1/2}$ ,  $y=(8Zr)^{1/2}$ ,  $J_s(y)$  is the Bessel function, and  $\kappa$  is the relativistic quantum number of the Dirac theory. For PD from an  $S$  state,  $j=1/2$  or  $3/2$ . We match the Dirac wave function for  $r<r_0$  at  $r=r_0$  to the solution  $\psi$  of the Pauli equation

$$\left( -\frac{1}{2}\nabla^2 + \hat{V} + \frac{1}{2c^2} \frac{1}{r} \frac{d\hat{V}}{dr} \mathbf{s}\cdot\mathbf{1} - E \right) \Psi = 0, \quad (30)$$

where  $\hat{V}$  is the operator (21) whose diagonal matrix elements are given by Eqs. (22) and (23).

The standard transformation for this purpose is [25,26]

$$\psi = (1 + \mathbf{p}^2/8c^2)\psi_A, \quad (31)$$

where  $\psi_A$  is the large component of the Dirac wave function and  $\mathbf{p}$  is the momentum operator. This transformation neglects  $V$  compared to  $c^2$ . The transformation (31) gives a Pauli wave function  $\psi$  which is only approximately normalized [25]. In contrast, if we do not neglect  $V/c^2$  (but disregard the nonrelativistic part  $E_{NR}$  of the total electron energy), Eq. (31) becomes

$$\psi = [1 + \boldsymbol{\sigma} \cdot \mathbf{p} f(r) \boldsymbol{\sigma} \cdot \mathbf{p}] \psi_A, \quad (32)$$

where  $f(r) = [8c^2(1 - V/2c^2)^2]^{-1}$ . By using standard properties of the Pauli matrices  $\boldsymbol{\sigma}$ , Eq. (32) can be rewritten as

$$\psi = \left( 1 - \frac{df}{dr} \frac{d}{dr} - f\nabla^2 + \frac{1}{r} \frac{df}{dr} \boldsymbol{\sigma} \cdot \mathbf{l} \right) \psi_A. \quad (33)$$

By separating spin and angular variables, we obtain the corresponding relation between the  $p$ -wave Pauli radial function  $u(r)$  and the large component of the Dirac radial function  $G(r)$ ,

$$u_j(r) = \left\{ 1 - r \frac{df}{dr} \frac{d}{dr} \frac{1}{r} - f \left[ \frac{d^2}{dr^2} - \frac{2}{r^2} \right] + \frac{1}{r} \frac{df}{dr} \left[ j(j+1) - \frac{11}{4} \right] \right\} G_\kappa(r). \quad (34)$$

After calculating  $u_j(r)$  in the  $jj$  representation, we recouple to the  $LS$  representation according to

$$u_{LSJ} = (-1)^{1+J-L} \sqrt{2S+1} \sum_{j=L-1/2}^{L+1/2} u_j \sqrt{2j+1} \begin{Bmatrix} L & J & S \\ \frac{1}{2} & \frac{1}{2} & j \end{Bmatrix} \quad (35)$$

and integrate the system

$$\left( \frac{d^2}{dr^2} - \frac{2}{r^2} + k^2 - 2V_{L=1,S}(r) - 2D_{SS}^1 v(r) \right) u_S(r) = 2D_{01}^1 v(r) u_{S'}(r) \quad (36)$$

of coupled radial Pauli equations numerically for  $r > r_0$ . The radial function  $u_S(r)$  was defined in Eq. (20). The diagonal and off-diagonal parts of the spin-orbit interaction appear on the left- and right-hand sides, respectively, of Eq. (36). The indices  $S$  and  $S'$  take values of 0 and 1, respectively, for the first equation, and 1 and 0, respectively, for the second equation. Furthermore, we write  $V_{so}$  as  $[v(r)\mathbf{s} \cdot \mathbf{l}]$  by defining

$$v(r) = \frac{1}{2c^2 r} \frac{dV_{L=1,S}}{dr}.$$

$D_{SS'}^1$  is the coupling matrix [cf. Eq. (24)]. The local potentials  $V_{L=1,S}$  describe the electron-atom interaction in chan-

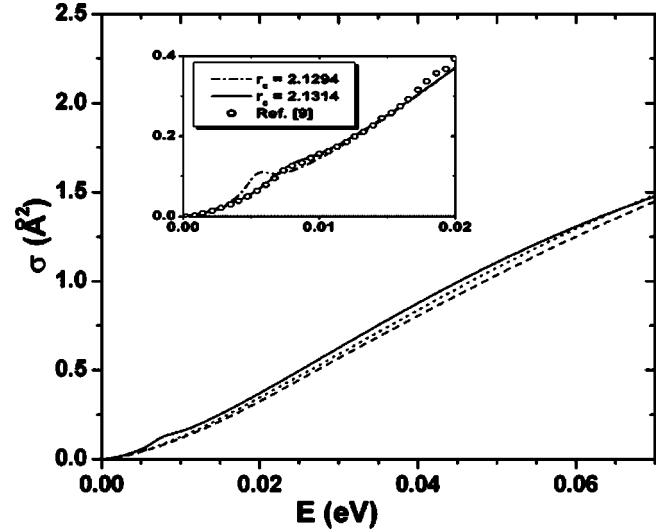


FIG. 1. Near-threshold PD cross section for  $\text{Rb}^-$  (dotted line),  $\text{Cs}^-$  (solid line), and  $\text{Fr}^-$  (dashed line). The inset shows our calculations based on the Dirac  $R$ -matrix data from Ref. [17] (dash-dotted line), and after fine-tuning the peak of the  $^3P_1^o$  resonance to 8 meV [21] (solid line). In the inset, our results for  $\text{Cs}^-$  are compared with the experimental data from Fig. 2 of Ref. [9] (normalized to our absolute PD cross section at 8 meV) for two slightly different values of the cutoff radius  $r_c$ .

nels  $^1P$  ( $V_{L=1,S=0}$ ) and  $^3P$  ( $V_{L=1,S=1}$ ). To assure Hermiticity of the spin-orbit interaction, we assume that  $dV_{L=1,S=0}/dr = dV_{L=1,S=1}/dr$  near the origin, where the spin-orbit interaction is important. Since the nuclear screening parameter  $\lambda$  is the same for  $V_{L=1,S=0}$  and  $V_{L=1,S=1}$ , this requirement is satisfied with a high accuracy.

## V. NUMERICAL RESULTS AND DISCUSSION

Figure 1 gives the total PD cross section  $\sigma = \sigma_0 + \sigma_1$  [where  $\sigma_0$  and  $\sigma_1$  are given by Eq. (18) for  $S=0$  and  $S=1$ , respectively], for energies of the photoelectron just above the detachment threshold of  $A^-$  ( $A$  stands for Rb, Cs, and Fr). Our calculations for Cs, based on the Dirac  $R$ -matrix results for eigenphases [17,18], exhibit a local peak whose position, 5.6 meV above the threshold, is somewhat lower than the observed peak at 8 meV [9], and the theoretical width of 2.7 meV is smaller than the experimental value of 5 meV. Therefore, we have tuned the position of the  $J=1$  resonance by changing the parameter  $r_c$  in Eq. (22) for the  $^3P^o$  symmetry from 2.1294 to 2.1314. This modification has shifted the position of the  $J=1$  resonance to 8 meV. The resulting curve, shown in the inset of Fig. 1, agrees with the experimental data from Fig. 2 of Ref. [9], with respect to both the resonance position and width. On the other hand, the  $^3P$  resonance contribution to PD of  $\text{Rb}^-$  and  $\text{Fr}^-$  is unnoticeable in Fig. 1, due to the dominating  $^1P$  background.

The  $^3P$  resonance appears due to a combination of the centrifugal barrier and the polarization potential. Therefore its position can be efficiently controlled by the cutoff parameter  $r_c$  entering the polarization potential. A slight increase of

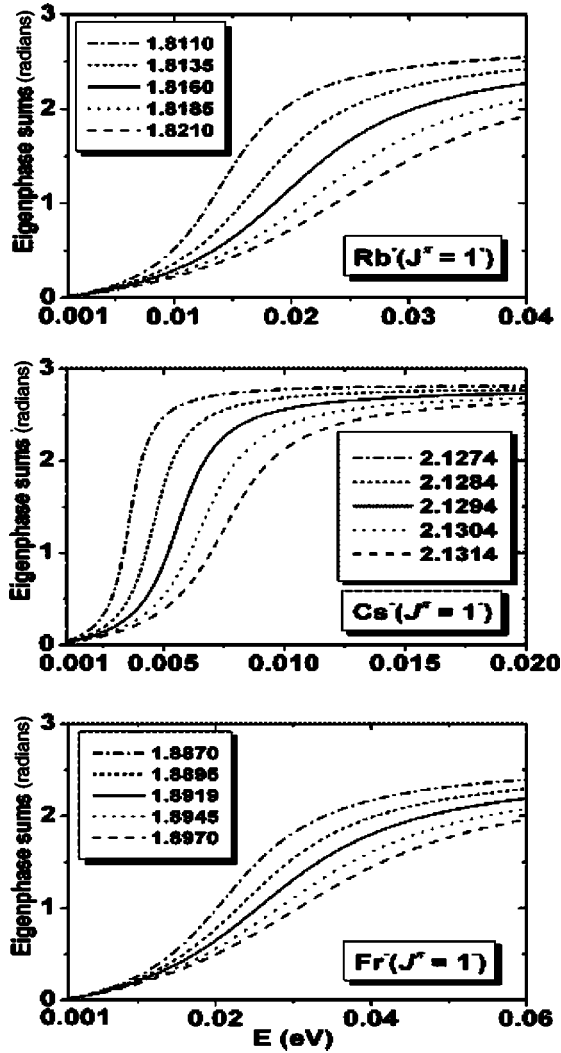


FIG. 2. Energy dependence of the eigenphase sums for the  $J^\pi = 1^-$  symmetry (where  $\pi$  is the parity) of  $\text{Rb}^-$ ,  $\text{Cs}^-$ , and  $\text{Fr}^-$  ions, for several values of  $r_c$  (indicated in the legend). In each graph, the solid line corresponds to the  $r_c$  value that gives the best fit of our Pauli eigenphase sums to the Dirac  $R$ -matrix results from Refs. [17,18] for  $\text{Rb}^-$  (1.8160),  $\text{Cs}^-$  (2.1294), and  $\text{Fr}^-$  (1.8919).

the parameter  $r_c$  in Eq. (22) produces a slightly less attractive electron-atom interaction and shifts the resonance position toward larger energies. For the  $\text{Cs}^-$  ion, an increase of the parameter  $r_c$  from 2.1294 to 2.1314 (by only 0.094%) produces a shift of about 2.4 meV in the position of the  $^3P$  resonance. The high sensitivity of the resonance position to  $r_c$  is due to the very low resonance energy close to the bound part of the negative ion spectrum. Indeed, as follows from Fig. 2, the resonance position and width are much more sensitive to  $r_c$  in the case of  $\text{Cs}^-$ , where the resonance occurs at a lower energy than for  $\text{Rb}^-$  and  $\text{Fr}^-$ .

In Fig. 3 we plot the  $^3P$  contributions to the total PD cross section for all three ions. The inset of Fig. 3 shows the agreement between our cross sections near the  $^3P_1^o$  resonance of  $\text{Cs}^-$  and the experimental data from Fig. 3 of Ref. [9]. For  $\text{Rb}$ , the  $^3P$  contribution is about 2.7 times lower than that for  $\text{Cs}$ , which is not surprising because of the

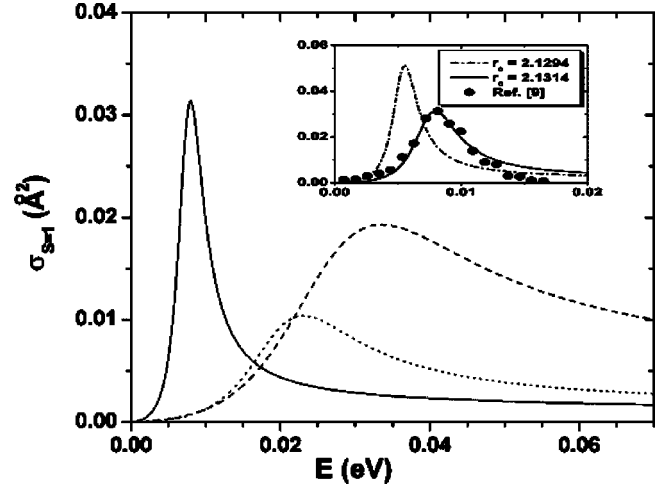


FIG. 3.  $^3P_1^o$  contribution to PD (shown in Fig. 1) for  $\text{Rb}^-$  (dotted line),  $\text{Cs}^-$  (solid line), and  $\text{Fr}^-$  (dashed line) ions. The inset shows the same comparison as Fig. 1, for the  $^3P_1^o$  contribution.

weaker spin-orbit interaction. However, for  $\text{Fr}$  the  $^3P$  contribution is lower than for  $\text{Cs}$  too, in spite of the higher nuclear charge. For a qualitative discussion and tentative explanation of this surprising effect, we note that the resonance contribution to the final-state wave function can be obtained by setting  $S=0$ ,  $S'=1$ , and by integrating Eq. (36),

$$u_0(r) = \int G(r, r') \frac{1}{\sqrt{2}c^2 r'} \frac{dV_{L=1, S=1}}{dr'} u_1(r') dr'. \quad (37)$$

In Eq. (37),  $G(r, r')$  is the Green's function of the radial Hamiltonian on the left-hand side of Eq. (36). In lowest order of perturbation theory, we drop the spin-orbit interaction term in  $G(r, r')$ . Since  $dV_{L=1, S=1}/dr'$  in Eq. (37) is proportional to the nuclear charge  $Z$ , we expect the matrix element (16) for the triplet scattering state to be approximately proportional to  $Z\bar{u}_1$ , where  $\bar{u}_1$  is a typical value for the resonant part of the radial wave function. In consequence, according to Eq. (17), the detachment cross section is expected to behave as  $Z^2\bar{u}_1^2$ .

To estimate  $\bar{u}_1$ , we use the following result for the resonance part of the scattering wave function [32]  $\psi = a\phi$ , where the function  $\phi$  is normalized to 1, and the absolute value of  $a$  is given by (we assume that  $\psi$  is normalized to the  $\delta$  function of momentum)

$$|a|^2 = \frac{k\Gamma}{2\pi[(E - E_{res})^2 + \Gamma^2/4]}. \quad (38)$$

At the resonance,  $E = E_{res}$  and  $|a|^2 = 2(2E_{res})^{1/2} / [\pi\Gamma(E_{res})]$ . For the  $P$  resonance  $\Gamma \propto E^{3/2}$  and therefore the peak value of  $|a|^2$  scales as  $1/E_{res}$ . In Fig. 4, we present numerically calculated radial wave functions for  $J=0$  at energies corresponding to resonance positions (19.2, 4.0, and 13.2 meV for  $\text{Rb}$ ,  $\text{Cs}$ , and  $\text{Fr}$ , respectively). Since there is only one open channel for  $J=0$ , we discuss the  $J=0$  instead of the  $J=1$  term. This will not affect our conclusions below.

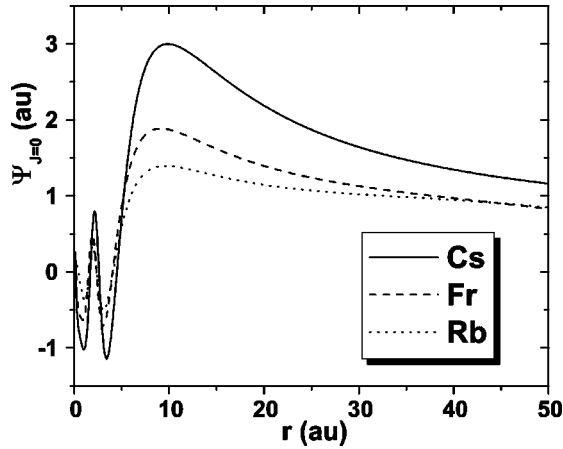


FIG. 4. Numerically calculated radial wave functions for  $J=0$  at energies corresponding to resonance positions (19.2, 4.0, and 13.2 meV for Rb, Cs, and Fr, respectively).

The wave functions in Fig. 4 have their maximum at distances of about 12 a.u., and then decay into the classically forbidden region due to the potential barrier formed by the centrifugal potential. As shown in Table II, the peak value scales as  $E_{res}^{-1/2}$  in accordance with our result for  $|a|$ . Consequently, the triplet contribution to the cross section scales as  $Z^2/E_{res}$  within a factor of 2. For Fr, the larger value of  $Z$  is offset by a larger value of  $E_{res}$ . Therefore scaling for the peak value at  $J=0$  works better than scaling for the PD cross section. In addition, the  $^1P$  background contribution for Fr is larger at  $E=E_{res}$  because of the larger value of  $E_{res}$ . Strictly speaking, this scaling works only for very narrow resonances; therefore deviations from this simple law are substantial, especially for the cross section. However, it allows us to understand our results qualitatively.

The accuracy of our present PD results is mainly indicated by the precision of the Dirac eigenphases computed in [17,18] and used in this model. The accuracy of the Dirac scattering eigenphases was discussed in Ref. [17], and, for Fr, is limited by the electron affinities (EAs) we have used in our Dirac  $R$ -matrix calculations. For Rb and Cs atoms, accurate experimental EAs are available. For Fr atoms, no experimental EA is available, and we have estimated its value at 492 meV within a 2% error [17]. A detailed discussion regarding the consequences of this uncertainty for the characteristics of the  $^3P^o$  resonance was given in [17], and the results are shown in Fig. 3 of Ref. [17]. The uncertainty in the position of the  $J=1$  component of the  $\text{Fr}^- (^3P^o)$  resonance (at 24 meV) was estimated to be 23% (about 6 meV).

TABLE II. Parameters derived from the numerical study of the wave function for  $J=0$  at the resonance position  $E_{res}$ . To help the reader to understand Fig. 4, we also show the turning points  $r_1$  and  $r_2$  for the classical motion of the electron in the superposition of the centrifugal and polarization potentials.

Atom	$E_{res}$ (meV)	$u_{max}$ (a.u.)	$u_{max}\sqrt{E_{res}}$	$[10^4\sigma(\text{\AA}^2)]E_{res}/Z^2$	$r_1$ (a.u.)	$r_2$ (a.u.)
Rb	19.2	1.3930	6.10	1.55	13.54	35.13
Cs	4.0	2.9960	5.99	0.83	14.41	81.21
Fr	13.2	1.8839	6.84	0.61	13.17	43.45

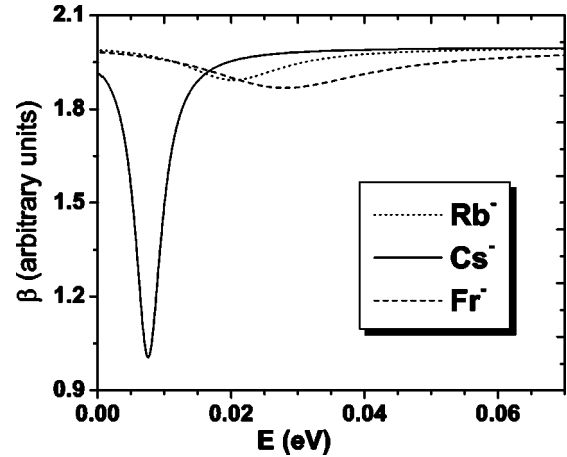


FIG. 5. Asymmetry parameters as functions of the energy of the photodetached electron for PD of  $\text{Rb}^-$  (dotted line),  $\text{Cs}^-$  (solid line), and  $\text{Fr}^-$  (dashed line).

This uncertainty is not significantly changed by the fitting procedure we use in order to get the Pauli eigenphases from the Dirac eigenphases. It remains indicative for the accuracy of our PD results for Fr.

We conclude that the  $^3P$  contributions to the total PD cross sections for Rb and Fr are too small to be noticeable. However, the differential cross sections and the asymmetry parameter  $\beta$  [33] are more sensitive to the  $^3P$  contribution. In the angular distribution of photoelectrons [Eq. (17)], the  $S=1$  contribution adds a  $\sin^2\theta$  term to the pure  $\cos^2\theta$  dependence of the  $S=0$  contribution. Therefore, the asymmetry parameter in the angular distribution [34],

$$\frac{d\sigma}{d\Omega} = \frac{\sigma[1 + \beta P_2(\cos\theta)]}{4\pi}, \quad (39)$$

differs from its maximum value 2. In Eq. (39), both the angle-integrated,  $\sigma$ , and the angle-differential,  $d\sigma/d\Omega$ , PD cross sections include the summation over the final spin  $S=0$  and 1 states.  $P_2(\cos\theta)$  is the Legendre polynomial for  $l=2$ , and  $\theta$  is the polar angle of the unit vector  $\hat{k}$  in Eq. (17). Figure 5 shows the energy dependence of the  $\beta$  parameter for  $\text{Rb}^-$ ,  $\text{Cs}^-$ , and  $\text{Fr}^-$  ions, while Fig. 6 presents our angle-differential cross section (DCS) results for PD of  $\text{Rb}^-$ . In comparison with the similar result for  $\text{Cs}^-$  (see Fig. 2 in Ref. [21]), the  $^3P$  contribution for  $\text{Rb}^-$  near  $\theta$  of  $90^\circ$  is much less pronounced. This is mainly due to a much broader  $^3P$  resonance for  $\text{Rb}^-$  than for  $\text{Cs}^-$ . We also note that our DCS for  $\text{Rb}^-$  at  $\theta=90^\circ$  (of  $0.0016 \text{\AA}^2/\text{rad}$ ) is only 2% of the DCS at



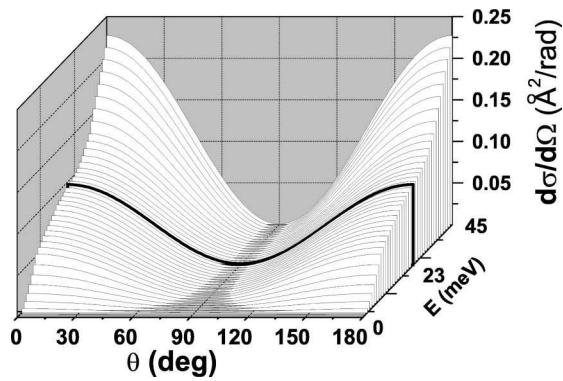


FIG. 6. The angle-differential PD cross section near the detachment threshold for  $\text{Rb}^-$ . The  $^3P$  contribution has a maximum at about 23 meV, indicated by the thick line.

$\theta = 180^\circ$ . This percentage is very small compared with that for  $\text{Cs}^-$  of about 24%. For  $\text{Cs}^-$ , the DCS at  $90^\circ$  is  $0.005 \text{ \AA}^2/\text{rad}$ . For  $\text{Fr}^-$ , the DCS results are similar to those for  $\text{Rb}^-$ . These results are not surprising, since the minimum of the  $\beta$  parameter is 1.89 (1.87) for  $\text{Rb}^-$  ( $\text{Fr}^-$ ), which is a weak deviation from  $\beta_{\max} = 2$ . For  $\text{Cs}^-$ , the deviation is more important, since  $\beta_{\min} = 1$ .

The present results can be used as a guideline for future experimental attempts to detect the  $^3P^o$  resonance in heavy alkali-metal anions. Measurements of the  $\beta$  parameter have

already been done by Frey *et al.* [8] in single-photon PD of  $\text{Rb}^-$ , in the region of the  $\text{Rb}(5p^2P_{1,2,3/2})$  thresholds. Frey *et al.* carefully tested the accuracy of this technique in order to identify resonances. We hope that our results will stimulate further experiments in the still unexplored spectral region near the  $\text{Rb}^-$  and  $\text{Fr}^-$  detachment thresholds.

## VI. SUMMARY

In conclusion, we have formulated boundary conditions for solving the Pauli equation, which are important for the description of the spin-orbit interaction effects in electron scattering and PD processes. The application of this method to the near-threshold PD of  $\text{Cs}^-$  allows us to calculate the contribution of the  $^3P_1^o$  resonance in very good agreement with the experimental results in [9].

For  $\text{Rb}^-$  and  $\text{Fr}^-$  we predict this contribution to be very small and therefore not easily observable in total PD cross section measurements. However, the  $^3P_1^o$  resonance contribution leaves a clear signature in the  $\beta$  parameters, and therefore will be better accessible in measurements of angle-differential PD cross sections for  $\text{Rb}^-$  and  $\text{Fr}^-$ .

## ACKNOWLEDGMENT

This work was supported by the Science Division, Office of Fusion Energy Sciences, Office of Energy Research, U.S. Department of Energy.

- 
- [1] C.-N. Liu and A.F. Starace, *Phys. Rev. A* **59**, 3643 (1999); C.-N. Liu, *ibid.* **64**, 052715 (2001).
- [2] N. Vinci, D.H. Glass, K.T. Taylor, and P.G. Burke, *J. Phys. B* **33**, 4799 (2000).
- [3] G. Haeffler, I.Yu. Kiyani, U. Berzinsh, D. Hanstorp, N. Brandefelt, E. Lindroth, and D.J. Pegg, *Phys. Rev. A* **63**, 053409 (2001); K.T. Andersson, J. Sandström, I.Yu. Kiyani, D. Hanstorp, and D.J. Pegg, *ibid.* **62**, 022503 (2000); I.Yu. Kiyani, U. Berzinsh, J. Sandstrom, D. Hanstorp, and D.J. Pegg, *Phys. Rev. Lett.* **84**, 5979 (2000).
- [4] D.W. Norcross, *Phys. Rev. A* **7**, 606 (1973).
- [5] D.L. Moores and D.W. Norcross, *Phys. Rev. A* **10**, 1646 (1974).
- [6] C.H. Greene, *Phys. Rev. A* **42**, 1405 (1990).
- [7] T.A. Patterson, H. Hotop, A. Kasdan, D.W. Norcross, and W.C. Lineberger, *Phys. Rev. Lett.* **32**, 189 (1974).
- [8] P. Frey, F. Breyer, and H. Hotop, *J. Phys. B* **11**, L589 (1978); P. Frey, M. Lawen, F. Breyer, H. Klar, and H. Hotop, *Z. Phys. A* **304**, 155 (1982).
- [9] M. Scheer, J. Thogersen, R.C. Bilodeau, C.A. Brodie, H.K. Haugen, H.H. Andersen, P. Kristensen, and T. Andersen, *Phys. Rev. Lett.* **80**, 684 (1998).
- [10] I.I. Fabrikant, *J. Phys. B* **19**, 1527 (1986).
- [11] U. Thumm and D.W. Norcross, *Phys. Rev. Lett.* **67**, 3495 (1991); *Phys. Rev. A* **45**, 6349 (1992).
- [12] I.I. Fabrikant, *Opt. Spektrosk.* **53**, 131 (1982) [*Opt. Spectrosc.* **53**, 131 (1982)]; J.L. Krause and R.S. Berry, *Comments At. Mol. Phys.* **18**, 91 (1986); C. Froese Fischer and D. Chen, *J. Mol. Struct.* **199**, 61 (1989).
- [13] I.I. Fabrikant, *Phys. Rev. A* **45**, 6404 (1992).
- [14] K. Bartschat, *J. Phys. B* **26**, 3595 (1993).
- [15] V.M. Borodin, I.I. Fabrikant, and A.K. Kazansky, *Phys. Rev. A* **44**, 5725 (1991); V.M. Borodin and A.K. Kazansky, *J. Phys. B* **25**, 971 (1992).
- [16] I.I. Fabrikant, *Comments At. Mol. Phys.* **32**, 267 (1996).
- [17] C. Bahrim and U. Thumm, *Phys. Rev. A* **61**, 022722 (2000).
- [18] C. Bahrim, U. Thumm, and I.I. Fabrikant, *Phys. Rev. A* **63**, 042710 (2001).
- [19] A.R. Johnston and P.D. Burrow, *J. Phys. B* **15**, L745 (1982).
- [20] S.J. Buckman and Ch.W. Clark, *Rev. Mod. Phys.* **66**, 539 (1994).
- [21] C. Bahrim, I.I. Fabrikant, and U. Thumm, *Phys. Rev. Lett.* **87**, 123003 (2001); **88**, 109904(E) (2002).
- [22] H.A. Bethe and E.E. Salpeter, *Quantum Mechanics of One- and Two-Electron Systems* (Springer, Berlin, 1957).
- [23] E.U. Condon and G.H. Shortley, *The Theory of Atomic Spectra* (Cambridge University Press, Cambridge, England, 1935).
- [24] J.-L. Heully, I. Lindgren, E. Lindroth, S. Lundqvist, and A.-M. Mårtensson-Pendrill, *J. Phys. B* **19**, 2799 (1986); Ch. Chang, M. Pelissier, and Ph. Durand, *Phys. Scr.* **34**, 394 (1986); W. Kutzelnigg, *Z. Phys. D: At. Mol. Clusters* **11**, 15 (1989); *Phys. Rev. A* **54**, 1183 (1996); E. van Lenthe, E.J. Baerends, and J.G. Snijders, *J. Chem. Phys.* **99**, 4597 (1993).
- [25] J.J. Sakurai, *Advanced Quantum Mechanics* (Addison-Wesley, Reading, MA, 1967).
- [26] V.B. Berestetskii, E.M. Lifshitz, and L.P. Pitaevskii, *Relativistic Quantum Theory* (Pergamon, Oxford, 1971).

- [27] A.F. Starace, Phys. Rev. A **3**, 1242 (1971); **8**, 1141 (1973); M.Ya. Amusia, N.A. Cherepkov, L.V. Chernysheva, and S.I. Sheftel, Phys. Lett. **28A**, 726 (1969).
- [28] C. Bottcher and A. Dalgarno, Proc. R. Soc. London, Ser. A **340**, 187 (1974); G. Peach, J. Phys. B **11**, 2107 (1978); P. Valiron, R. Gayet, R. McCarroll, F. Masnou-Seeuws, and M. Philippe, *ibid.* **12**, 53 (1979); C. Laughlin and G.A. Victor, Adv. At. Mol. Phys. **25**, 163 (1988).
- [29] P. Swan, Proc. R. Soc. London, Ser. A **228**, 10 (1955).
- [30] J.N. Bardsley, Case Stud. At. Phys. **4**, 299 (1974).
- [31] The radius  $r_0$  is of the order of 0.01 a.u. and should not be confused with the much larger  $R$ -matrix radius of 40 a.u.
- [32] U. Fano, Phys. Rev. **124**, 1866 (1961).
- [33]  $\beta$  is a measure of the deviation of the photoelectron distribution from isotropy ( $\beta=0$ ), and completely characterizes the shape of the emission pattern.
- [34] S.T. Manson and A.F. Starace, Rev. Mod. Phys. **54**, 389 (1982).